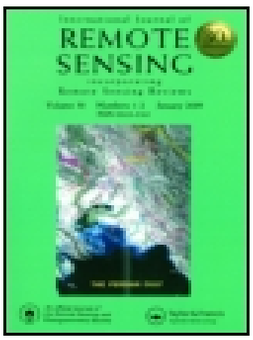

International Journal of Remote Sensing

ISSN: 0143-1161 (Print) 1366-5901 (Online) Journal homepage: http://www.tandfonline.com/loi/tres20

Scale transformation of Leaf Area Index product retrieved from multiresolution remotely sensed data: analysis and case studies

Xin Tao , Binyan Yan , Kai Wang , Daihui Wu , Wenjie Fan , Xiru Xu & Shunlin Liang

To cite this article: Xin Tao , Binyan Yan , Kai Wang , Daihui Wu , Wenjie Fan , Xiru Xu & Shunlin Liang (2009) Scale transformation of Leaf Area Index product retrieved from multiresolution remotely sensed data: analysis and case studies, International Journal of Remote Sensing, 30:20, 5383-5395, DOI: 10.1080/01431160903130978

To link to this article: http://dx.doi.org/10.1080/01431160903130978

Published online: 30 Sep 2009.

International Journal of Remote Sensing
Vol. 30, No. 20, 20 October 2009, 5383–5395

Taylor & Francis
Taylor & Francis Group

Scale transformation of Leaf Area Index product retrieved from multiresolution remotely sensed data: analysis and case studies

XIN TAO†‡, BINYAN YAN†, KAI WANG§, DAIHUI WU†, WENJIE FAN*†, XIRU XU† and SHUNLIN LIANG‡

†Institute of Remote Sensing and GIS, Peking University, Beijing 100871, PR China
‡Department of Geography, University of Maryland, College Park, Maryland 20742, USA
§State Key Laboratory of Remote Sensing Science, Jointly Sponsored by the Institute of Remote Sensing Applications of Chinese Academy of Sciences and Beijing Normal University, Beijing 100101, PR China

Climate and land–atmosphere models rely on accurate land-surface parameters, such as Leaf Area Index (LAI). It is crucial that the estimation of LAI represents actual ground truth. Yet it is known that the LAI values retrieved from remote sensing images suffer from scaling effects. The values retrieved from coarse resolution images are generally smaller. Scale transformations aim to derive accurate leaf area index values at a specific scale from values at other scales. In this paper, we study the scaling effect and the scale transformation algorithm of LAI in regions with different vegetation distribution characteristics, and analyse the factors that can affect the scale transformation algorithm, so that the LAI values derived from a low resolution dataset match the average LAI values of higher resolution images. Using our hybrid reflectance model and the scale transformation algorithm for continuous vegetation, we have successfully calculated the LAI values at different scales, from reflectance images of 2.5 m and 10 m spatial resolution SPOT-5 data as well as 250 m and 500 m spatial resolution MODIS data. The scaling algorithm was validated in two geographic regions and the results agreed well with the actual values. This scale transformation algorithm will allow researchers to extend the size of their study regions and eliminate the impact of remote sensing image resolution.

1. Introduction

Leaf Area Index (LAI), used globally to monitor plant density and quality, serves as an important input parameter in many climate and land–atmosphere models (Bonan *et al*. 1993). Yet it has been widely reported that differences in image resolution influence LAI calculations (Rastetter *et al.* 1992, Friedl 1997, Walsh *et al*. 1997). The values retrieved from coarse spatial resolution images are generally smaller than those based on higher spatial resolution images. This scaling phenomenon results from the nonlinearity of the retrieving functions as well as spatial heterogeneity (Li and Strahler 1986, Chen 1999, Liang 2000, Tian *et al.* 2002, Garrigues *et al.* 2006, Tao *et al.* 2008, Xu *et al.* 2009).

The LAI can be derived directly from reflectance data or from vegetation indices. Because most vegetation indices suffer from scaling effects (Friedl 1997, Walsh *et al.* 1997), parameters based on these vegetation indices suffer from multiple scaling

*Corresponding author. Email: fanwj@pku.edu.cn

International Journal of Remote Sensing
ISSN 0143-1161 print/ISSN 1366-5901 online
http://www.tandf.co.uk/journals
DOI: 10.1080/01431160903130978

effects and any subsequent interactions. In order to avoid such complications, we retrieve LAI values directly from reflectance data. The calculations of LAI for discrete and continuous vegetation differ, so they have different scaling effects. In this paper, we focus on continuous vegetation, which is horizontally homogeneous, and has indistinct individual texture (Liang 2004, Xu 2005). Using remote sensing images of various resolutions, we study scaling effects and apply the algorithm proposed by Xu *et al.* (2009) for transforming values derived from remote sensing images at different scales. We are able to map LAI from low resolution data so that model results match the mean values from higher resolution images. This method is validated in two geographic regions with different vegetation distribution characteristics. The validation results indicate very good matches with ground measurements. Using this algorithm, we can map LAI over large areas more accurately using low resolution data (Townshend *et al.* 1988).

2. LAI retrieval and scaling analysis

2.1 *LAI retrieval formulas*

The reflectance of continuous vegetation is the sum of single scattering and multiple scattering, $\rho = \rho^1 + \rho^m$, where ρ^1 means the contribution of single scattering, and ρ^m represents the contribution of multiple scattering. The contribution of multi-scattering can be expressed by Hapke's model (Hapke 1981, Lacaze and Roujean 2001, Lacaze *et al.* 2002, Xu *et al.* 2009). The formula for calculating ρ^1 is (Nilson and Kuusk 1989, Xu 2005, Jin *et al.* 2007a, 2007b):

$$\begin{aligned}\rho^1 = \rho_g &\left\{ e^{-\lambda_0\left[\frac{G_S}{\mu_s}+\frac{G_V}{\mu_V}-\frac{G_V}{\mu_V}\Gamma(\phi)\right]LAI} + \left[e^{-\lambda_0\frac{G_V}{\mu_V}LAI} - e^{-\lambda_0\left[\frac{G_S}{\mu_s}+\frac{G_V}{\mu_V}-\frac{G_V}{\mu_V}\Gamma(\phi)\right]LAI}\right]\frac{E_d}{\mu_0 F_0 + E_d}\right\} \\ &+ \rho_v\left\{\left(1 - e^{-\lambda_0\frac{G_V}{\mu_V}LAI\cdot\Gamma(\phi)}\right) + \left[e^{-\lambda_0\frac{G_V}{\mu_V}LAI\cdot\Gamma(\phi)} - e^{-\lambda_0\frac{G_V}{\mu_V}LAI}\right]\frac{E_d}{\mu_0 F_0 + E_d}\right\},\end{aligned} \tag{1}$$

where ρ_g and ρ_v are the hemispherical albedos of the soil background and the vegetation respectively; λ_0 is the Nilson parameter accounting for the vegetation clumping effect; μ_s and μ_v are cosine values of the solar and viewing zenith angle; G_s and G_v are the mean projection of a unit foliage area along the solar and viewing direction respectively. $G_{s,v} = \frac{1}{2\pi}\int_{2\pi} g_L(\Omega_L)\left|\Omega_L \cdot \Omega_{s,v}\right| d\Omega_L$, where $1/2\pi \cdot g_L(\Omega_L)$ is the probability density of the distribution of the leaf normals with respect to the upper hemisphere, i.e. Leaf Angle Distribution (LAD) (Liang 2004). The empirical function $\Gamma(\phi)$ describes the hot-spot phenomenon, where the symbol ϕ accounts for the sun-target-sensor position and depends on the angle between the solar and viewing direction and the LAD of canopy. When $0 \le \phi \le \pi$, $\Gamma(\phi) = 1 - \phi/\pi$. E_d is the diffuse irradiance from sky scattering; $\mu_0 F_0$ is the direct irradiance from solar illumination.

This equation includes reflective anisotropic characteristics caused by sun-target-sensor geometry and neglects reflective anisotropic characteristics caused by soil background and leaf canopy. Field validation shows that the model can simulate the canopy BRDF accurately (Liu *et al.* 2008). In the hot-spot direction, the variable ϕ=0 and $\Gamma(0) = 1$, so that the equation can be reduced to

$$\rho^1 = \rho_g e^{-\lambda_0\frac{G_V}{\mu_V}LAI} + \rho_v\left(1 - e^{-\lambda_0\frac{G_V}{\mu_V}LAI}\right). \tag{2}$$

Substituting b for $\lambda_0\frac{G_v}{\mu_v}$,

$$\rho^1 = \rho_g e^{-b \cdot LAI} + \rho_v \left(1 - e^{-b \cdot LAI}\right) \tag{3}$$

According to the analysis of Xu *et al.* (2009), equation (3) can be used to study the LAI scaling effect.

2.2 *Definition of scale*

In remote sensing applications, spatial scale corresponds to the pixel resolution. The concepts of relative scale and scale order were proposed by Xu *et al.* 2009. The concept of relative scale r_R is expressed as

$$r_R = {}^{r}/_{r_0}, \tag{4}$$

where r is the pixel resolution and r_0 is the spatial resolution of a zero-order scale pixel. Within a zero-order scale pixel the spatial distribution of components is approximately homogenous. The proportion of mixed pixels can be neglected in an image totally constituted of zero-order scale pixels. We call this image zero-order scale image. If the ratio of two adjacent order scales is a constant d, called scale base, then

$$r_R = d^n (\text{or } n = \log_d r_R). \tag{5}$$

Leaf area index is defined as one half the total green leaf area per unit horizontal ground surface area (Chen and Black 1992). In equation (5), when scale order $n = 0$, pixel resolution $r = r_0$, the retrieved LAI at this scale order is denoted by LAI_0. At this order of scale, almost no mixed pixels exist, vegetation in the pixel is homogenous, and the LAI measured on this scale can represent the true condition of vegetation growth. When $n \geq 1$, LAI_n denotes the value of LAI at n-order scale. If there is heterogeneity, such as soil in the pixel, the retrieved LAI fails to characterize the vegetation growth condition exactly (Xu *et al.* 2009).

2.3 *Scaling formulas for LAI*

Suppose an n-order scale pixel is comprised of M pixels at zero-order scale, and the number of the fully-covered vegetation pixels is m (see figure 1 where $M = 9$ and $m = 8$). Ignoring the growth difference among the vegetation pixels, the projected proportion of vegetation area for the n-order scale pixel is $\frac{m}{M}\left(1 - e^{-b \cdot LAI_0}\right)$ according to the Boolean projection principle. The projected proportion of vegetation area can be remotely sensed. When we observe the pixel at n-order scale, we can only assume that vegetation is homogeneous in it, and calculate the LAI at this scale, thus

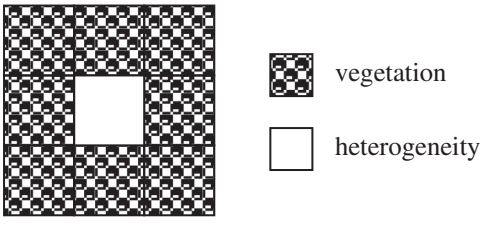

Figure 1. The composition of an n-order scale pixel by several zero-order scale pixels.

$$1 - e^{-b \cdot \mathrm{LAI}_n} = \frac{m}{M}\left(1 - e^{-b \cdot \mathrm{LAI}_0}\right). \tag{6}$$

If the vegetation proportion is denoted by $a_{\mathrm{v}}(n)$, we obtain the relationship between LAI_n and LAI_0

$$b \cdot \mathrm{LAI}_n = -\ln\left\{1 - a_{\mathrm{v}}(n)\left[1 - e^{-b \cdot \mathrm{LAI}_{0,\mathrm{a}}}\right]\right\}, \tag{7}$$

where $a_{\mathrm{v}}(n)$ is actually the proportion of vegetation in the target vegetation pixel at n-order scale. $\mathrm{LAI}_{0,\mathrm{a}}$ represents the corresponding true LAI value averaged in the extent of the target n-order scale vegetation pixel. It is exactly the same as the formula derived from the relationships between adjacent order scales (Xu *et al.* 2009), in which $a_{\mathrm{v}}(n)$ is expressed as:

$$a_{\mathrm{v}}(n) = a_{\mathrm{v},n} a_{\mathrm{v},n-1,\mathrm{a}} \cdots a_{\mathrm{v},1,\mathrm{a}}. \tag{8}$$

The symbol $a_{v,n}$ is the vegetation pixel proportion at $n-1$-order scale included in the target n-order scale pixel. The symbol $a_{\mathrm{v},i,\mathrm{a}}$, $i = 1, \ldots, n-1$, represents the value averaged in the extent of the target n-order scale pixel, of vegetation pixel proportion at the $i-1$-order scale included in the i-order scale pixel. The function of $a_{\mathrm{v}}(n)$ can be calculated using (Xu *et al.* 2009):

$$a_{\mathrm{v}}(n) = \frac{1-c}{e^{pn}} + c, \tag{9}$$

where c and p are empirically determined constants, $0 \leq c \leq 1$ and $p \geq 0$. These two constants determine the range and rate of the scaling effect.

2.4 *Scaling analysis*

In order to study the determinants of constants c and p, numerical simulations were conducted. In a synthetic image, the number of heterogeneity patches is gradually increased from 300 to 700 to 1000, as shown in figures 2(*b*)–2(*d*). The relationships between $a_{\mathrm{v}}(n)$ and scale are shown in figure 2(*a*), where 'heterogeneity num' denotes the number of heterogeneity patches. With the increase of heterogeneity, the descending of $a_{\mathrm{v}}(n)$ is more obvious, and the c value decreases from 0.92, 0.82 to 0.73. It is understandable that since c has a positive relationship with $a_{\mathrm{v}}(n)$, representing the proportion of vegetation, it also has a positive relationship with the vegetation cover. On the other hand, it is obvious that the descending rate of $a_{\mathrm{v}}(n)$ accelerates with the increase of heterogeneity patches, but calculations show that the three curves all share the same p value, 0.1165. It is concluded that c depends on the total area of heterogeneity while p depends on some element other than the number of heterogeneity patches.

In another synthetic image with a size of 1024×1024, we broke the heterogeneity patches in it into smaller ones, from 32×32, to 16×16, to 8×8, as shown in figures 3(*b*)–3(*d*). We obtained similar relationships between $a_{\mathrm{v}}(n)$ and scale, as shown in figure 3(*a*), where the heterogeneity size denotes the size of heterogeneity patches. With the decrease of heterogeneity patch sizes, the descending rate of $a_{\mathrm{v}}(n)$ gradually accelerates, and p increases from 0.0619, 0.1165, to 0.1863. As $a_{\mathrm{v}}(n)$ converges at a smaller scale, the decreasing rate of $a_{\mathrm{v}}(n)$ is faster, and the value of p becomes bigger. It is concluded that p depends on the size of heterogeneity. If the total area of heterogeneity is fixed, then the smaller the heterogeneity patch, the larger the p value. In the real world, different sizes of heterogeneity coexist and the dominant size determines the value of p.

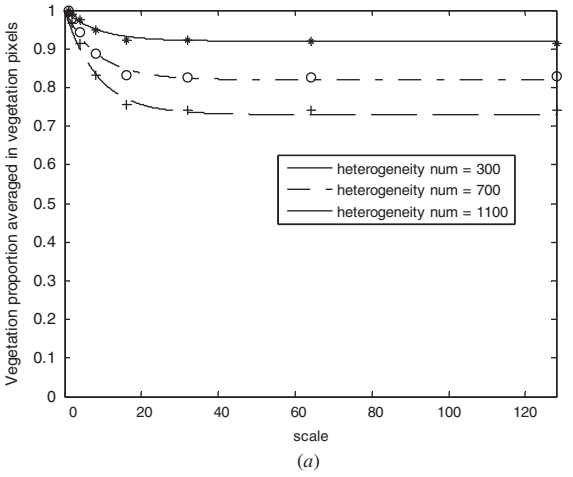

(*a*)

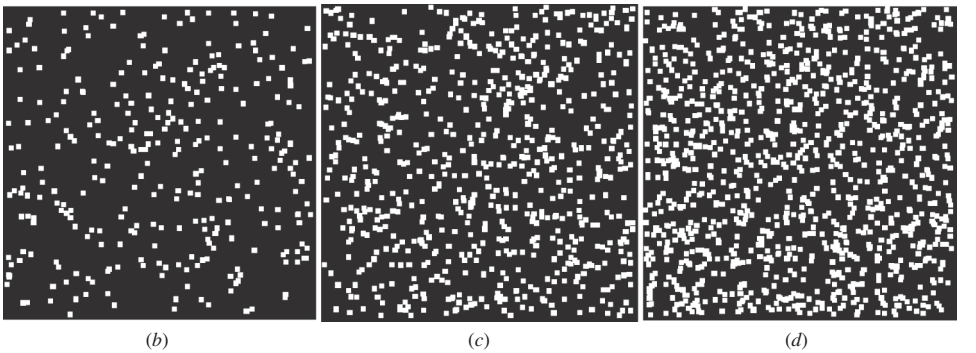

(*b*) (*c*) (*d*)

Figure 2. (*a*) The curves of a_v descending with scale when heterogeneity patches gradually increase; (*b*) synthetic image where heterogeneity number is 300; (*c*) synthetic image where heterogeneity number is 700; (*d*) synthetic image where heterogeneity number is 1100.

We now need to add the factor of vegetation growth, which contributes to LAI variance. This allows us to calculate the final value of acquired $\mathrm{LAI}^*_{0,a}$ using (Xu *et al.* 2009):

$$\mathrm{LAI}^*_{0,a} = \mathrm{LAI}_{0,a} + m \cdot V_{\mathrm{LAI},0}, \tag{10}$$

where $\mathrm{LAI}_{0,a}$ is derived from equation (7) and represents the mean value of the true LAIs, m is empirically determined and equals 0.3589 in our experiments, and $V_{\mathrm{LAI},0}$ is the variance of $\mathrm{LAI}_{0,i}$ at zero-order scale. The LAI variance can be derived from the first and the second order scales (Xu *et al.* 2009):

$$V_{\mathrm{LAI},0} = \frac{V^2_{\mathrm{LAI},1}}{V_{\mathrm{LAI},2}}. \tag{11}$$

Equation (7) can be rewritten as:

$$e^{-b\cdot \mathrm{LAI}_n} = 1 - \left[e^{-pn}(1-c) + c\right]\left(1 - e^{-b\cdot \mathrm{LAI}_{0,a}}\right). \tag{12}$$

For a specific region, vegetation proportion and distribution are determinant, so equation (12) can be further rewritten as:

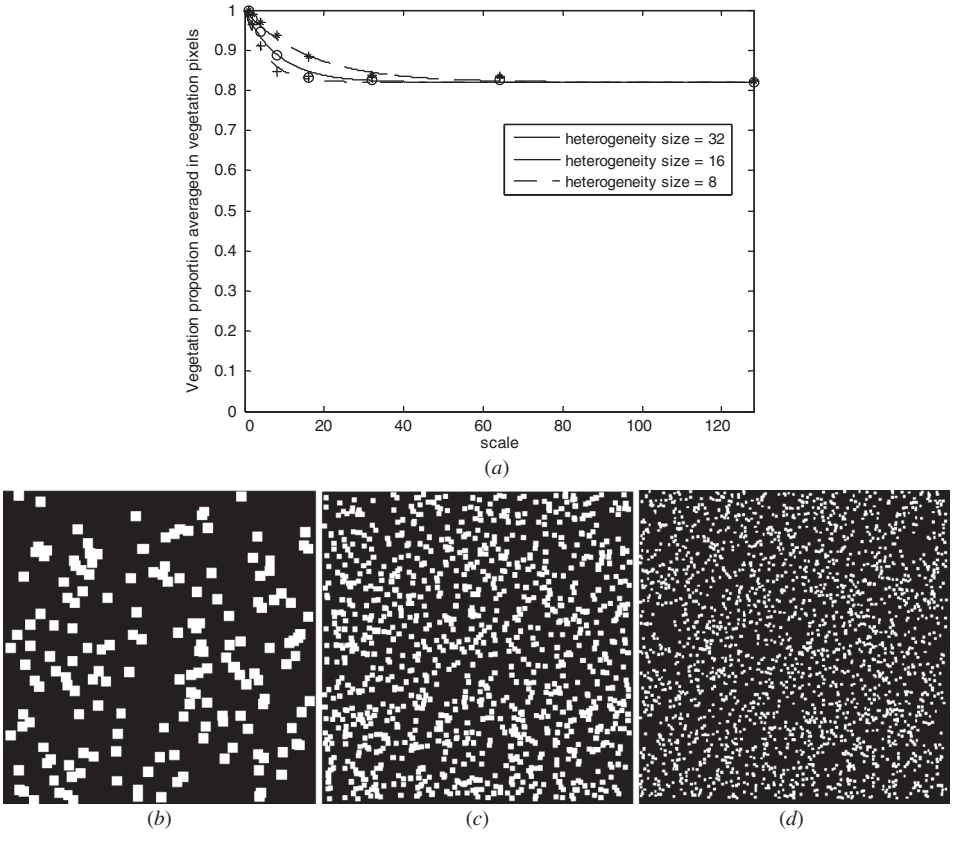

Figure 3. (*a*) The curves of a_v descending with scale when heterogeneity patches are broken up; (*b*) synthetic image where heterogeneity size is 32 × 32; (*c*) synthetic image where heterogeneity size is 16 × 16; (*d*) synthetic image where heterogeneity size is 8 × 8.

$$e^{-b\cdot \mathrm{LAI}_n} = (1 - D) - B \cdot e^{-pn} \tag{13}$$

$$B = (1 - c)\left(1 - e^{-b\cdot \mathrm{LAI}_{0,a}}\right) \tag{14}$$

$$D = c\left(1 - e^{-b\cdot \mathrm{LAI}_{0,a}}\right) \tag{15}$$

The relationship between LAI_n and scale order n is approximately negatively linear (Xu *et al.* 2009).

3. Case studies of scaling transform applications

3.1 *Remote sensing images of the study regions*

In order to analyse the mechanism of the LAI scaling effect in actual remote sensing images, we chose two study regions with different characteristics of vegetation distribution. The first region is of 60 km × 34 km in Jining City, Shandong Province, northern China, within the geographic region of 115°52′ E–117°52′ E, 34°26′ N–35°57′ N. The images were acquired on 6 May 2005. The vegetation is mostly winter wheat, which has a continuous spatial distribution in the region, and the vegetation patch is large. The

second is a region of 17 km × 13 km, located at Putian City, Fujian Province, southern China, within the geographic region of 118°27′ E–119°40′ E, 24°59′ N–25°46′ N. The images were acquired on 9 November 2006. Vegetation is primarily rice which is scattered in the region and the vegetation patch is small. We used remote sensing images at four spatial resolutions in these two regions. Two SPOT-5 images for each region were purchased from Spot Image Corporation: a panchromatic image at a resolution of 2.5 m and a multispectral image at 10 m. Two MODIS multispectral images, at 250 m and 500 m resolutions, were downloaded from the MODIS website.

The SPOT-5 images were preprocessed for radiometric calibration, atmospheric correction and geometric correction. Atmospheric correction was handled by 6S (the Second Simulation of Satellite Signal in the Solar Spectrum), version 4.1 (Vermote *et al.* 1997). We chose a mid-latitude atmospheric model and continental aerosols model. The visibility for the aerosol model concentration was 20 km, from meteorological data. In addition, cross-radiation correction was performed on both SPOT-5 images to eliminate interactions among adjacent pixels. This was done using the edge method, and the point spread function (PSF) was directly obtained from the image (Liu *et al.* 2004). Finally, another image at 50 m resolution was generated by linearly resampling the pixels of the 10 m SPOT-5 image. Geometric corrections were applied to the MODIS reflectance products using MRT software. The final reflectance images of the two study regions at five scales are shown in figure 4.

The next process applied is supervised classification using the maximum likelihood method on these images at different scales. The main land cover categories in the study regions are continuous vegetation (primarily winter wheat in Jining and rice in Putian), towns, roads, water bodies and aqueducts. The classification was performed so that vegetation and heterogeneity pixels were separated from remote sensing images.

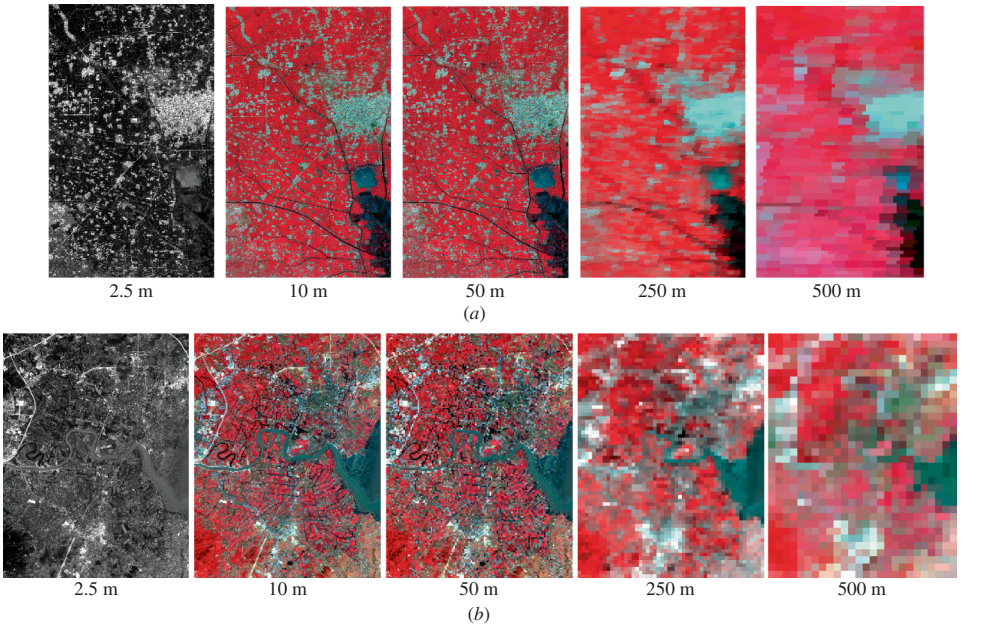

Figure 4. Reflectance images of the two study regions at five scales, in (*a*) Jining; (*b*) Putian (R: infrared, G: red, B: green).

3.2 *LAI retrieval and scaling effects*

Considering the differences of sun-target-sensor geometries both among pixels and images, equation (1) and the Hapke model were used to calculate LAI in vegetation pixels at each scale for the two regions.

These formulas require the recognition of pure vegetation and pure background reflectance. They were read out from the John Hopkins University spectral library. We need to solve for three values: λ_0, ϕ and LAI. To solve the equations, we applied the least square method to the band data of each multispectral image. Accordingly we obtained LAI distributions at four scales. Since the values of ϕ and λ_0 are similar in corresponding sites, we use every ϕ and λ_0 derived above to describe relevant 2.5 m resolution panchromatic pixels (Jin *et al.* 2007a, 2007b), and finally succeeded in calculating LAI values of 2.5 m resolution panchromatic pixels. The LAI distribution maps at five scales in Jining are shown in figure 5. In these images, the region showing a strong red hue has a relatively higher LAI value and the black region represents non-vegetation. Clearly, the LAI value derived from remote sensing images decreases as the scale increases.

Considering the 2.5 m SPOT-5 LAI distribution image to be a zero-order scale image, let scale base $d = 3$, then the scale orders of 10 m, 50 m, 250 m and 500 m resolution images are calculated to be 1.26, 2.73, 4.19 and 4.82, respectively. Beginning with the region included in the 500 m spatial resolution vegetation pixel, we calculated the mean of LAI at each scale order. The LAI mean value at 4.82-order scale is simply the retrieval LAI value calculated using formula (1) and the Hapke model. The mean value at any other scale order is the average of the retrieval LAI values of vegetation pixels at corresponding resolution. As shown in figure 6, with the increase of n, the LAI mean at n-order scale gradually decreases, approximating a negative correlation relationship.

Studying the region included in the whole image, we calculated the mean LAI at each scale order. These analogous calculations produced the same results. Again we observed a negative correlation relationship (the two grey lines in figure 6). The relationship between LAI_n and scale order n is approximately negatively linear, which matches our former mathematical analysis. Because the function of $a_v(n)$ is based on the statistical mean, and the values of c vary with pixels, some of the curves in figure 6 depart from negative linearity.

We note that the range of scaling effects, i.e. the decrease of LAI from 0-order scale to 4.82-order scale, is smaller in Jining than that in Putian. As we discussed above, this

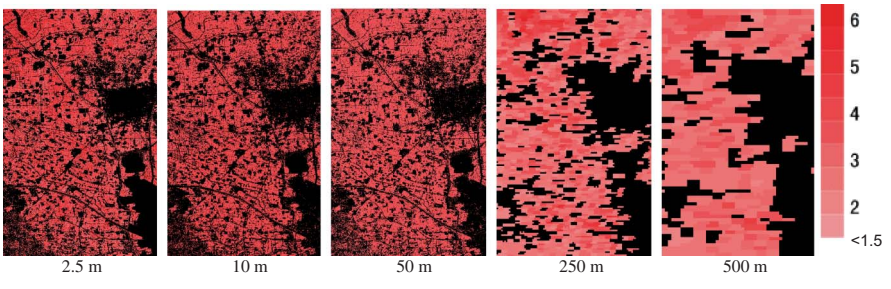

Figure 5. LAI distributions at five scales in Jining. The black region represents non-vegetation.

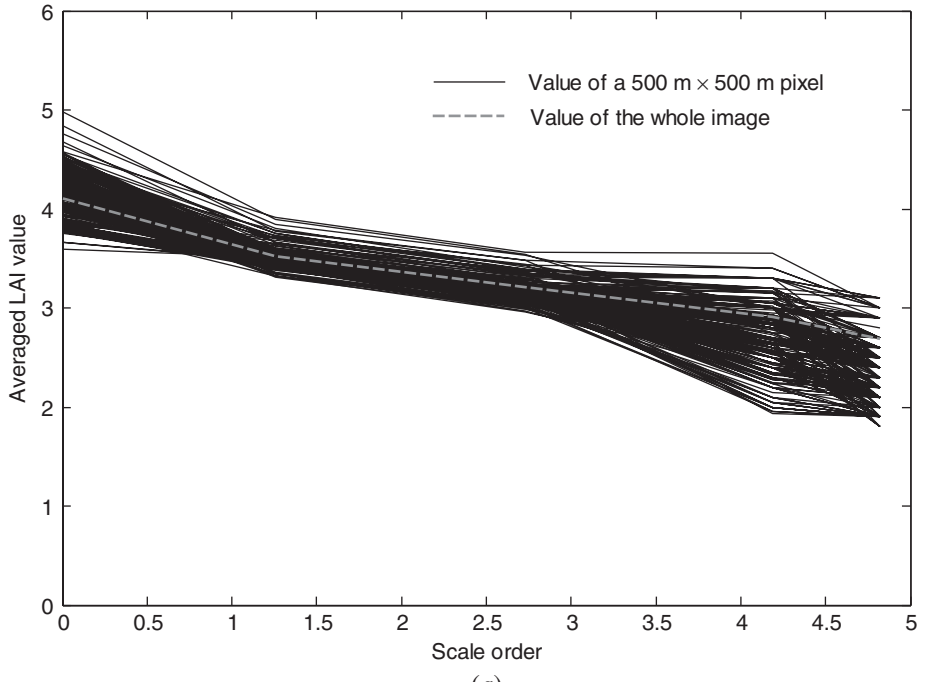

(*a*)

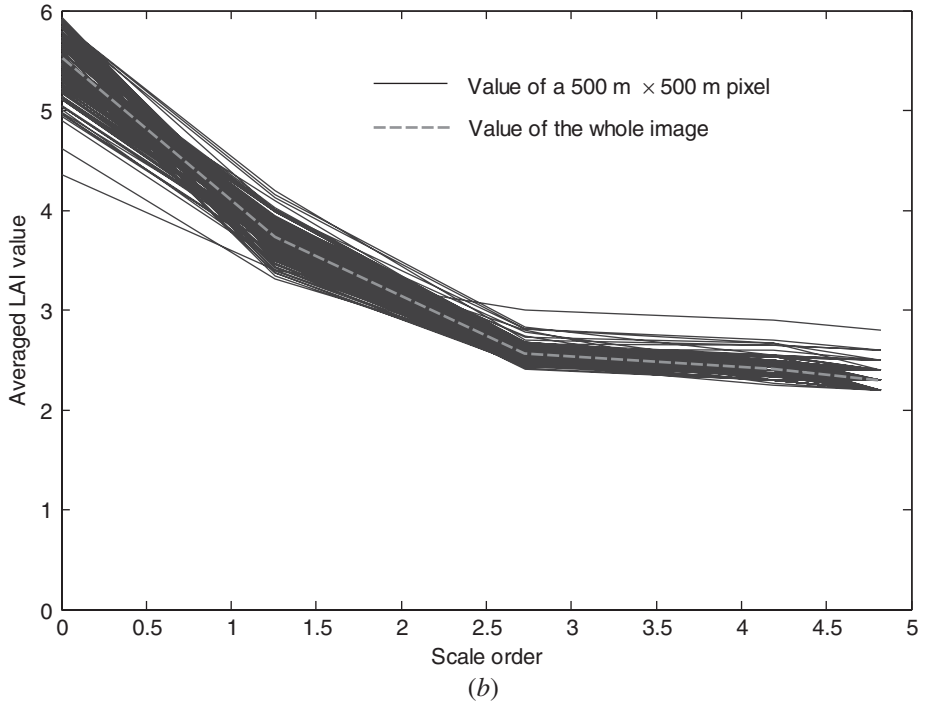

(*b*)

Figure 6. The mean value of LAI at each scale order in (*a*) Jining; (*b*) Putian.

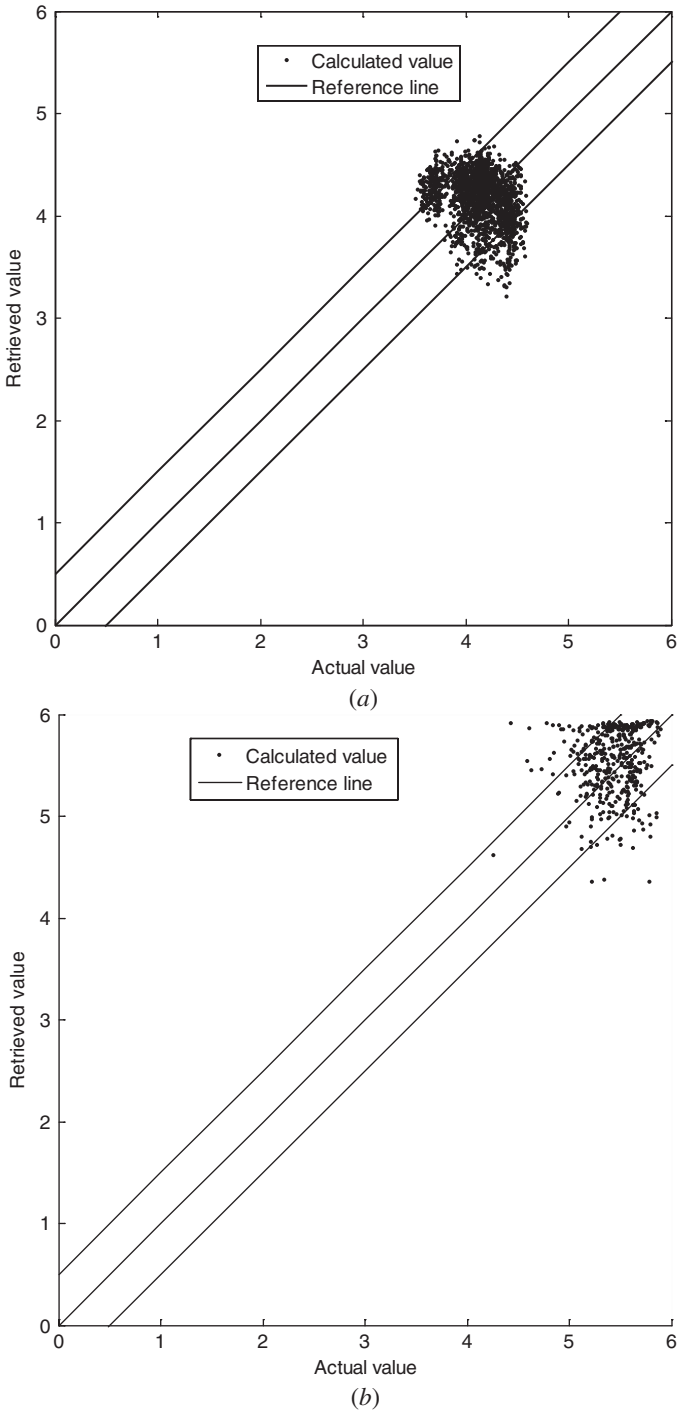

Figure 7. Comparisons of retrieval LAI and ground truth in (*a*) Jining; (*b*) Putian. The three reference lines in the figure have a slope of 45°. The middle line in the figure passes through the origin, meaning that points along it have no error. The other two lines are shifted up and down 0.5 units, points on it indicating some error with an absolute value of 0.5.

Table 1. The absolute errors for scaling transform of LAI.

	Average error	Maximum error	Minimum error	Standard deviation of errors
Jining	0.4426	1.2921	0	0.3319
Putian	0.4581	1.6687	0.0001	0.4723

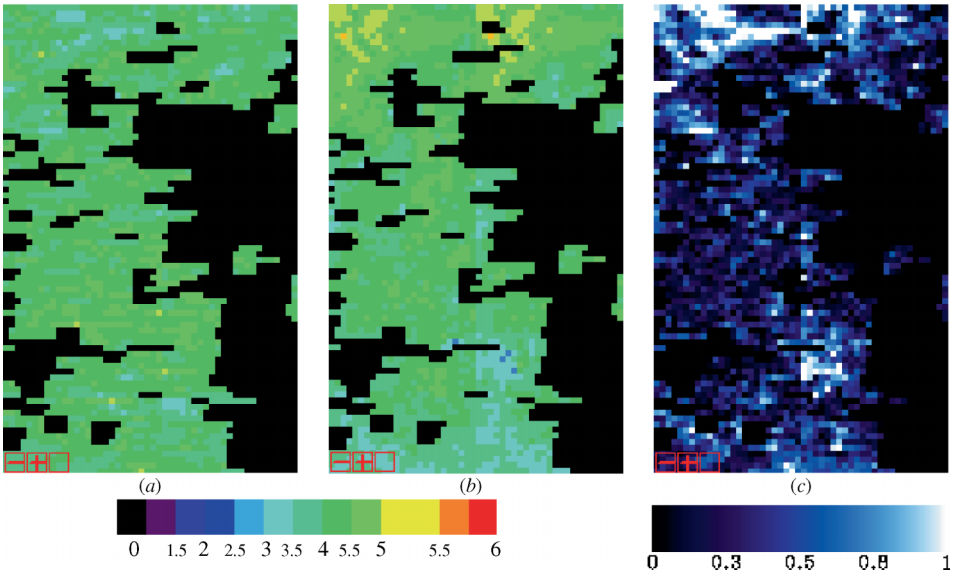

Figure 8. Comparison of LAI scaling transform value and actual value in Jining. The black represents non-vegetation. (*a*) The distribution of LAI calculated using scaling transform formula; (b) the distribution of LAI calculated from 0-order scale image; (c) the distribution of error.

is caused by the larger vegetation proportion in Jining. The decrease of LAI with scale is slower in Jining than that in Putian, and this can be explained by less heterogeneity.

3.3 *Scale transformation applications*

Again we consider 2.5 m spatial resolution to be zero-order scale, and suppose LAI at this scale to be unknown. We aim to derive the LAI mean value at this scale for each 500 m $\times$ 500 m vegetation pixel, from LAI values at four scales: 10 m and 50 m SPOT-5 as well as 250 m and 500 m MODIS. Looking at equations (7) and (8), or equation (12), we need to solve for three values, $LAI_{0,a}$, c and p, where c and p are constants. To solve these equations, we applied the least square method to the data at the four scales. Comparisons of retrieved values and actual values of *LAI* at zero-order scale are shown in figure 7.

Referring to figure 7, most points are constrained between the two lines shifted up and down 0.5 units from the origin, showing that the calculations match well with the actual LAI values that represent ground truth. Retrieval errors are shown in table 1.

For further comparison, we put three images together: the distribution of LAI calculated using scale transformation formula, the distribution of LAI calculated from zero-order scale image, and the distribution of error. They are shown in figure 8.

4. Conclusions

LAI scaling effects produce differences in the retrieval values at various scales. The purpose of scale transformation is to derive accurate average LAI values of zero-order scale from values at other scales. Zero-order scale of a remote sensing image indicates that inhomogeneous vegetation can be ignored within each pixel; the LAI value at this scale is considered to be the true LAI.

Both mathematical deduction and remote sensing image experiments show that LAI at n-order scale (LAI_n) decreases with scale n. This result agrees with the analyses of some other research (Chen 1999, Liang 2000, Garrigues *et al*. 2006). The range and rate of the scaling effect of LAI is determined by the vegetation area proportion as well as the size of the heterogeneity patch. The range of the scaling effect is large if the vegetation area proportion is low. When the vegetation area proportion is fixed, the decreasing rate of the scaling effect accelerates if the size of the heterogeneity patch becomes smaller.

With the scale transformation formula of LAI, we have succeeded in deriving the average LAI value at zero-order scale from LAI values at other scales. The calculation agrees well with actual LAI values. The scaling formula is derived for continuous cover vegetation. Researchers studying such vegetation may expand the size of the region they study by using lower resolution images and still produce valid results.

Acknowledgements

This paper was supported by the Special Funds for Major State Basic Research Project (Grant No. 2007CB714402), the National Natural Science Foundation of China (Grant No. 40871186 and No. 40401036) and National High-Tech Development Program (Grant No. 2005AA133011XZ07). We would like to thank the MODIS team for making available the reflectance products to the public freely, the referees for helpful suggestions and Miss Huiran Jin for the earlier work. We also thank Drs Murrel and Coral for the English edit.

References

Bonan, G.B., Pollard, D. and Thompson, S.L., 1993, Influence of subgrid-scale heterogeneity in leaf area index, stomatal resistance and soil moisture on grid-scale land-atmosphere interactions. *Journal of Climatology*, **6**, pp. 1882–1897.

Chen, J.M., 1999, Spatial scaling of a remotely sensed surface parameter by contexture. *Remote Sensing of Environment*, **69**, pp. 30–42.

Chen, J.M. and Black, T.A., 1992, Defining leaf area index for non-flat leaves. *Plant Cell and Environment*, **15**, pp. 421–429.

Friedl, M.A., 1997, Examining the effects of sensor resolution and sub-pixel heterogeneity on vegetation spectral indices: implications for biophysical modelling. In *Scale in Remote Sensing and GIS*, D.A. Quattrochi and M.F. Goodchild (Eds), pp. 113–139 (Boca Raton, FL: Lewis).

Garrigues, S., Allard, D., Baret, F., and Weiss., M., 2006, Influence of landscape spatial heterogeneity on the non-linear estimation of leaf area index from moderate spatial resolution remote sensing data. *Remote Sensing of Environment*, **105**, pp. 286–298.

HAPKE, B., 1981, Bidirectional reflectance spectroscopy: 1 Theory. *Journal of Geophysical Research*, **86**, pp. 3039–3054.

JIN, H., TAO, X., FAN, W., XU, X., and LI, P., 2007a, Monitoring the spatial distribution of high-resolution leaf area index using observations from DMC+4. In *Proceedings of International Geoscience and Remote Sensing Symposium*, 23–27 July 2007, Barcelona, Spain, pp. 3681–3684 (Institute of Electrical and Electronics Engineers).

JIN, H., TAO, X., FAN, W., XU, X., and LI, P., 2007b, Monitoring the spatial distribution of high-resolution Leaf Area Index using DMC+4 image. *Progress in Natural Science*, **17**, pp. 1229–1234 (in Chinese).

LACAZE, R. and ROUJEAN, J.L., 2001, G-function and HOt SpoT (GHOST) reflectance model application to multi-scale airborne POLDER measurements. *Remote Sensing of Environment*, **76**, pp. 67–80.

LACAZE, R., CHEN, J., ROUJEAN, J.L., and LEBLANC, S.G., 2002, Retrieval of vegetation clumping index using hot spot signatures measured by POLDER instrument. *Remote Sensing of Environment*, **79**, pp. 84–95.

LI, X. and STRAHLER, A.H., 1986, Geometric-optical bidirectional reflectance modeling of a coniferous forest canopy. *IEEE Transactions on Geoscience and Remote Sensing*, **24**, pp. 906–919.

LIANG, S., 2000, Numerical experiments on the spatial scaling of land surface albedo and leaf area index. *Remote Sensing Reviews*, **19**, pp. 225–242.

LIANG, S., 2004, *Quantitative Remote Sensing of Land Surfaces* (New Jersey: Wiley-Interscience).

LIU, X., FAN, W., TIAN, Q., and XU, X., 2008, Comparative analysis among different methods of leaf area index inversion. *Acta Scientiarum Naturalium Universitatis Pekinensis*, **44**, pp. 827–834.

LIU, Z., WANG, C. and LUO, C., 2004, Estimation of CBERS-1 point spread function and image restoration. *Journal of Remote Sensing*, **8**, pp. 234–237.

NILSON, T. and KUUSK, A., 1989, A reflectance model for the homogeneous plant canopy and its inversion. *Remote Sensing of Environment*, **27**, pp. 157–167.

RASTETTER, E.B., KING, A.W., COSBY, B.J., HORNBERGER, G.M., O'NEILL, R.V. and HOBBIE, J.E., 1992, Aggregating fine-scale ecological knowledge to model coarser-scale attributes of ecosystems. *Ecological Applications*, **2**, pp. 55–70.

TAO, X., YAN, B., WU, D., FAN, W., and XU, X., 2008, A scale transform method for Leaf Area Index retrieved from multi-resolutions remote sensing data. In *Proceedings of the 8th International Symposium on Spatial Accuracy Assessment in Natural Resources and Environmental Sciences*, J. Zhang and M.F. Goodchild (Eds.), 25–27 June 2008, Shanghai, China, pp. 176–182 (World Academic Union Ltd).

TIAN, Y.H., WOODCOCK, C.E. and WANG Y.J., 2002, Multiscale analysis and validation of the MODIS LAI product I. Uncertainty assessment. *Remote Sensing of Environment*, **83**, pp. 414–430.

TOWNSHEND, J.R.G. and JUSTICE, C.O., 1988, Selecting the spatial resolution of satellite sensors required for global monitoring of land transformations. *International Journal of Remote Sensing*, **9**, pp. 187–236.

VERMOTE, E.F., TANRE, D., DEUZE, J.L., HERMAN, M., and MORCRETTE, J.J., 1997, Second simulation of the satellite signal in the solar spectrum, 6S: An overview. *IEEE Transactions on Geoscience and Remote Sensing*, **35**, pp. 675–686.

WALSH, S.J., MOODY, A., ALLEN, T.R., and BROWN, D.G., 1997, Scale dependence of NDVI and its relationship to mountainous terrain. In *Scale in Remote Sensing and GIS*, D.A. Quattrochi and M.F. Goodchild (Eds), pp. 27–55 (Boca Raton, FL: Lewis).

XU, X., 2005, *Physics of Remote Sensing*, pp. 47–49 (Bejing: Peking University).

XU, X., FAN, W. and TAO, X., 2009, The spatial scaling effect of continuous canopy Leaves Area Index retrieved by remote sensing. *Science in China Series D-Earth Sciences*, **52**, pp. 393–401.